

Impact of PN junction inhomogeneity on the piezoelectric fields of acoustic waves in piezo-semiconductive fibers

Kai Fang^a, Peng Li^a, Nian Li^a, Dianzi Liu^b, Zhenghua Qian^{a,*}, Vladimir Kolesov^c, Iren Kuznetsova^c

^a State Key Laboratory of Mechanics and Control of Mechanical Structures, College of Aerospace Engineering, Nanjing University of Aeronautics and Astronautics, Nanjing 210016, China

^b School of Engineering, University of East Anglia, Norwich, UK

^c Kotelnikov Institute of Radio Engineering and Electronics of RAS, Moscow 125009, Russia



ARTICLE INFO

Keywords:

Piezoelectric semiconductor
Variable cross section
PN junction

ABSTRACT

Non-uniform mechanical strain can be easily induced at the interface of a piezoelectric semiconductive (PS) PN junction with variable cross sections by using piezoactive acoustic waves, and thus produces a giant piezoelectric field to significantly enhance the piezotronic effect. For revealing the piezotronic performance modulation in the non-uniform PS PN junction, the electromechanical field under a pair of applied end mechanical forces is studied from perspectives of theoretical analysis and numerical simulations. A one-dimensional linearized model for the PS fiber is established, which is applied for the mechanical analysis of a selected profile with the cross section varying in a specific quadratic function. Numerical results indicate that the acoustoelectric fields in the space charge region of the non-uniform PS PN junction are more sensitive to the applied mechanical forces, compared with that of the uniform junction, especially for a heterogeneous PN junction. Furthermore, the current-voltage relations of a necking PS PN junction can be modulated more easily by the end mechanical forces. Both qualitative conclusions and quantitative results can offer guidance for the piezotronic device design.

1. Introduction

Owing to the unique coupling of piezoelectricity and semiconductor properties, piezoelectric semiconductor (PS) materials are attracting tremendous attention in recent years [1–5]. Accompanying with that, more and more PS devices based on piezoactive acoustic waves are successfully developed and applied, such as nanogenerators [6,7], piezotronic field-effect transistors [8,9], piezotronic and chemical sensors [10,11], piezotronic logic nanodevices [12], piezotronic acoustic tweezers [13] and so forth. As known, semiconductor heterostructures are able to generate broadband or monochromatic coherent acoustic phonons with ultra-high frequency [4,14]. This is because that the space charge density of the semiconductor screens the piezoelectric field and instantaneously modifies the lattice equilibrium.

As one of the most important components in semiconductor devices, PN junction, made of a n-type semiconductor with electrons as majority carriers and a p-type semiconductor with holes, is usually encountered during device design and application. Physically, near the interface of the two type semiconductors, holes (electrons) are driven from the p-

zone (n-zone) to the n-zone (p- zone), forming a space charge region usually called depletion layer, whose width and height are two key parameters for the current–voltage relation of a PN junction [15]. Different from the conventional PN junction, the characteristics of PS PN junctions can be manipulated by applied mechanical loading, which is the novel advantage of PS materials and thus becomes a hotspot issue in piezotronics [16,17]. For example, the research work from Liu et al [18] concerns the current–voltage characteristics of a PS PN junction after considering the piezo-charges distribute at the interface within a small width. Luo et al [19] used the linearized method to deal with the nonlinearity in the electrons and holes current equations and investigated the electromechanical field distributions of the junction. Additionally, the exact theoretical solution in a piezoelectric PN junction subjected to a pair of tensile/compressive stresses is proposed by Fan et al [20] with the aid of multi-field coupling theory, and the modulation mechanism related to external forces are investigated in detail.

However, it should be stressed that the works conducted above are based on uniform PS fibers with flat profiles. To the author's knowledge, theoretical researches on non-uniform PS fibers with variable cross sections

* Corresponding author.

E-mail address: qianzh@nuaa.edu.cn (Z. Qian).

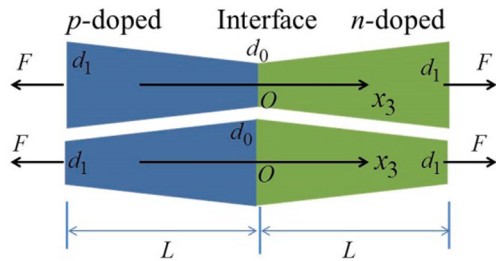


Fig. 1. Sketch of non-uniform PS PN junctions.

are relatively limited because of the mathematical challenge induced by the partial differential governing equations with variable coefficients [3,21,22], especially for a non-uniform PS PN junction. On the one hand, defects during mechanical processing can inevitably lead to a contoured profile with surface roughness. On the other hand, a non-uniform PS fiber with a variable cross section is sometimes designed, with the aim of capturing some higher performance indices. For instance, results displayed by Araneo et al [3] demonstrate that the PS fiber with a non-uniform strain gives substantially higher piezopotential and conversion efficiency and may increase the on-off ratios. Therefore, it is necessary to analyze the mechanical displacements of non-uniform PS materials that may be induced by piezoactive acoustic waves, which is the origin of this contribution.

Inspired by previous literatures [3,23], a non-uniform strain can be indeed produced in a non-uniform PS fiber with a contoured profile under the applied axial end mechanical forces due to piezoelectric effect. Therefore, the electromechanical fields of in a PS PN junction with variable cross sections are investigated in this paper, aiming at capturing higher sensitivity to the external mechanical force. Based on the fully coupled theory of PS materials [24–27], the linearized one dimensional model (1D) for the acoustic waves in non-uniform PS fibers is established in Section 2. Following that, the theoretical analysis of a specific PS PN junction with the area variation varying in a particular quadratic function is performed in Section 3. Here, the partial differential equation with variable coefficients has been transformed into the commonly used Helmholtz equation. After numerical validation, the working performances for homogeneous and heterogeneous junctions are compared in Section 4, and the merit of non-uniform PS fibers is revealed. Finally, some conclusions are drawn in Section 5. To some extent, the governing equation in the functionally graded (FG) PS materials has the same expression with the governing equation induced by a contoured profile [28]. Therefore, the methodologies in this paper, as well as the results illustrated here, are also suitable for an FG PS fiber.

2. Basic equations for acoustic waves of a 1D PS fiber with variable cross sections

As usual, a phenomenological, coupled-field theory for acoustic wave propagation consisting of the equations of linear piezoelectricity and charge conservation for electrons and holes can be adopted to describe dynamic behaviors of PS materials [29,30], i.e.,

$$\begin{aligned} \sigma_{ij,j} &= \rho \frac{\partial^2 u_i}{\partial t^2}, \\ D_{i,i} &= q(p - n + N_D^+ - N_A^-), \\ J_{i,i}^p &= -q \frac{\partial p}{\partial t}, \\ J_{i,i}^n &= q \frac{\partial n}{\partial t}, \end{aligned} \quad (1)$$

where σ_{ij} , u_i and D_i are the components of stress tensor, mechanical displacement vector, and electric displacement vector, respectively. The elementary charge $q = 1.6 \times 10^{-19}$ C, and ρ denotes mass density. p and

n respectively stand for the concentrations of holes and electrons, with J_i^p and J_i^n being their current densities. Correspondingly, N_D^+ and N_A^- are the impurity concentration of donors and acceptors. In this paper, a comma followed by a suffix denotes a material derivative operation, and the repeated subscript index implies a summation operation with respect to itself. In addition, it is assumed that the net recombination rate is zero in the continuity equations of carriers. The constitutive relations are as follows:

$$\begin{aligned} \sigma_{ij} &= c_{ijkl} S_{kl} - e_{kij} E_k, \\ D_i &= e_{ijk} E_j + e_{ijk} S_{jk}, \\ J_i^p &= qp \mu_{ij}^p E_j - q D_{ij}^p p_j, \\ J_i^n &= qn \mu_{ij}^n E_j + q D_{ij}^n n_j. \end{aligned} \quad (2)$$

Here S_{kl} and E_j are the components of strain tensor and electric field vector. c_{ijkl} , e_{ijk} , μ_{ij}^p (μ_{ij}^n) and D_{ij}^p (D_{ij}^n) represent the elastic stiffness constant, piezoelectric constants, dielectric constants, carrier mobility, and carrier diffusion constants, respectively. The generalized strain-displacement relation and the electric field-potential relation are:

$$\begin{aligned} S_{ij} &= \frac{1}{2}(u_{ij} + u_{ji}), \\ E_i &= -\varphi_i. \end{aligned} \quad (3)$$

The nonlinear terms in the last two equations of Eq. (2) makes it difficult to obtain an analytical solution. Employing the linearized method described in Refs. [31] and [32], the electron and hole concentrations in the piezoelectric semiconductors can be written as:

$$\begin{aligned} p &= p_0 + \Delta p, \quad n = n_0 + \Delta n, \\ p_0 &= N_A^-, \quad n_0 = N_D^+, \end{aligned} \quad (4)$$

where Δn and Δp are perturbations of the carrier concentrations, and n_0 and p_0 denote the carrier concentrations in the reference state before stress applied. This linearized method is acceptable when $|\Delta n| < 0.2n_0$ or $|\Delta p| < 0.2p_0$ [33], which will be followed in this paper. Considering the case of uniform doping with small Δp and Δn , some expressions in Eqs. (1) and (2) become:

$$\begin{aligned} D_{i,i} &= q(\Delta p - \Delta n), \\ q \frac{\partial}{\partial t} (\Delta p) &= -J_{i,i}^p, \\ q \frac{\partial}{\partial t} (\Delta n) &= J_{i,i}^n. \end{aligned} \quad (5)$$

$$\begin{aligned} J_i^p &= qp_0 \mu_{ij}^p E_j - q D_{ij}^p (\Delta p)_j, \\ J_i^n &= qn_0 \mu_{ij}^n E_j + q D_{ij}^n (\Delta n)_j. \end{aligned} \quad (6)$$

For a one-dimensional PS PN junction with a variable circular cross section shown in Fig. 1, the extensional deformation is considered in this paper, and then all the physical fields are independent of time. The whole length is $2L$ with equal n-type and p-type zones. For convinence, the x_3 coordinate locates along the central line of the fiber with its origin at the interface between n-type and p-type zones. d_0 and d_1 are the diameters of the interface and the end surface, respectively. The PS material is polarized along the axial direction and a pair of extensional forces F is applied at the two ends. For the equilibrium and the steady states considered, the governing equations become [34]:

$$\begin{aligned} (A\sigma_{33})_3 &= [A(\bar{c}_{33}u_{3,3} + \bar{e}_{33}\varphi_3)]_3 = 0, \\ (AD_3)_3 &= [A(\bar{e}_{33}u_{3,3} - \bar{e}_{33}\varphi_3)]_3 = -qA(\Delta n - \Delta p), \\ (AJ_3^n)_3 &= [A(-qn_0 \mu_{33}^n \varphi_3 + q D_{33}^n \Delta n_3)]_3 = 0, \\ (AJ_3^p)_3 &= [A(-qp_0 \mu_{33}^p \varphi_3 - q D_{33}^p \Delta p_3)]_3 = 0. \end{aligned} \quad (7)$$

Here A is the area of the cross section, which is dependent of x_3 . \bar{c}_{33} , \bar{e}_{33} and \bar{e}_{33} are the effective one-dimensional elastic, piezoelectric, and dielectric constants introduced by the one-dimensional stress relaxation condition [35], i.e.,

$$\begin{aligned}\bar{c}_{33} &= 1/s_{33}^E, \\ \bar{e}_{33} &= d_{33}/s_{33}^E, \\ \bar{e}_{33} &= e_{33}^T - d_{33}^2/s_{33}^E.\end{aligned}\quad (8)$$

The isolated boundary condition at two ends $x_3 = \pm L$ require zero currents, which leads to $J_3^n = J_3^p = 0$ in Eq. (7), and

$$\begin{aligned}\Delta n_{,3} &= n_0 \frac{\mu_{33}^n}{D_{33}^n} \varphi_{,3}, \\ \Delta p_{,3} &= -p_0 \frac{\mu_{33}^p}{D_{33}^p} \varphi_{,3}.\end{aligned}\quad (9)$$

Subtracting these two equations from each other, we get:

$$(\Delta n - \Delta p)_{,3} = \left(n_0 \frac{\mu_{33}^n}{D_{33}^n} + p_0 \frac{\mu_{33}^p}{D_{33}^p} \right) \varphi_{,3}. \quad (10)$$

The carried mobility $\mu_{33}^p (\mu_{33}^n)$ and the carrier diffusion constants $D_{33}^n (D_{33}^p)$ satisfy the Einstein relation:

$$\frac{\mu_{33}^n}{D_{33}^n} = \frac{\mu_{33}^p}{D_{33}^p} = \frac{q}{k_B T}. \quad (11)$$

where k_B is the Boltzmann constant and T represents the absolute temperature. The first equation in Eq. (7) indicates that the axial force $A\sigma_{33}$ is a constant. Meanwhile, the mechanical boundary conditions at $x_3 = \pm L$ require $A\sigma_{33} = F$, and then we can achieve

$$u_{3,3} = \frac{F}{\bar{c}_{33} A} - \frac{\bar{e}_{33}}{\bar{c}_{33}} \varphi_{,3} = \frac{F}{\bar{c}_{33} A} - \frac{\bar{e}_{33}}{\bar{c}_{33}} \frac{1}{n_0 \frac{\mu_{33}^n}{D_{33}^n} + p_0 \frac{\mu_{33}^p}{D_{33}^p}} (\Delta n - \Delta p)_{,3}. \quad (12)$$

Substituting Eq. (10) and Eq. (12) into the second equation of Eq. (7) yields

$$(\Delta n - \Delta p)_{,3} + \frac{A_3}{A} (\Delta n - \Delta p)_{,3} - \kappa^2 (\Delta n - \Delta p) = 0, \quad (13)$$

with

$$\kappa^2 = \frac{q(n_0 \frac{\mu_{33}^n}{D_{33}^n} + p_0 \frac{\mu_{33}^p}{D_{33}^p})}{\bar{e}_{33} (\frac{\bar{e}_{33}}{\bar{c}_{33} \bar{e}_{33}} + 1)}. \quad (14)$$

3. Analysis of electromechanical fields in a PS PN junction with a variational area

The area variation function of the PN junction shown in Fig. 1 is choosed as

$$A = A_0 (1 + \alpha \frac{x_3}{L})^2 \quad (15)$$

$$\begin{aligned}\Delta n - \Delta p &= \frac{\kappa' C_6 \sinh(\kappa' x_3) + \kappa' C_7 \cosh(\kappa' x_3)}{1 + \alpha \frac{x_3}{L}}, \varphi = \frac{\kappa' C_6 \sinh(\kappa' x_3) + \kappa' C_7 \cosh(\kappa' x_3)}{(n_0' \frac{\mu_{33}^{nl}}{D_{33}^{nl}} + p_0' \frac{\mu_{33}^{pl}}{D_{33}^{pl}})(1 + \alpha \frac{x_3}{L})} + C_8, \Delta n = n_0' \frac{\mu_{33}^{nl}}{D_{33}^{nl}} \frac{\kappa' C_6 \sinh(\kappa' x_3) + \kappa' C_7 \cosh(\kappa' x_3)}{(n_0' \frac{\mu_{33}^{nl}}{D_{33}^{nl}} + p_0' \frac{\mu_{33}^{pl}}{D_{33}^{pl}})(1 + \alpha \frac{x_3}{L})} + n_0' \frac{\mu_{33}^{nl}}{D_{33}^{nl}} C_8 + C_9, \Delta p \\ &= n_0' \frac{\mu_{33}^{nl}}{D_{33}^{nl}} \frac{\kappa' C_6 \sinh(\kappa' x_3) + \kappa' C_7 \cosh(\kappa' x_3)}{(n_0' \frac{\mu_{33}^{nl}}{D_{33}^{nl}} + p_0' \frac{\mu_{33}^{pl}}{D_{33}^{pl}})(1 + \alpha \frac{x_3}{L})} + n_0' \frac{\mu_{33}^{nl}}{D_{33}^{nl}} C_8 + C_9 - \frac{\kappa' C_6 \sinh(\kappa' x_3) + \kappa' C_7 \cosh(\kappa' x_3)}{1 + \alpha \frac{x_3}{L}}, u_3 \\ &= \frac{-F}{\bar{c}_{33}' A_0 (1 + \alpha \frac{x_3}{L})} \frac{L - \bar{e}_{33}'}{\bar{c}_{33}'} \frac{\kappa' C_6 \sinh(\kappa' x_3) + \kappa' C_7 \cosh(\kappa' x_3)}{(n_0' \frac{\mu_{33}^{nl}}{D_{33}^{nl}} + p_0' \frac{\mu_{33}^{pl}}{D_{33}^{pl}})(1 + \alpha \frac{x_3}{L})} - \frac{\bar{e}_{33}'}{\bar{c}_{33}'} C_8 + C_{10}.\end{aligned}\quad (24)$$

as an example, where A_0 is the cross section area at the interface $x_3 = 0$, and the coefficient α determines the area variation pattern. Admittedly, Eq. (15) can't represent a non-uniform PS PN junction with any arbitrary profile, but the investigation methodology proposed and results obtained in this paper are meaningful for the design of high-performance PS devices. With the aid of Eq. (15), Eq. (13) can be transformed into a Helmholtz equation [36,37], i.e.,

$$[(\Delta n - \Delta p)\psi]_{,33} - \kappa^2 (\Delta n - \Delta p)\psi = 0, \quad (16)$$

with

$$\psi = 1 + \alpha \frac{x_3}{L}. \quad (17)$$

In the following part of this paper, superscripts ' l ' and ' r ' respectively denote the quantities in the left and the right regions of the PN junction, i.e., $x_3 \leq 0$ and $x_3 \geq 0$. Taking the region $x_3 \geq 0$ for instance, the solution of Eq. (16) can be written as

$$(\Delta n - \Delta p)\psi^r = \kappa' C_1 \sinh(\kappa' x_3) + \kappa' C_2 \cosh(\kappa' x_3). \quad (18)$$

Then

$$\Delta n - \Delta p = \frac{\kappa' C_1 \sinh(\kappa' x_3) + \kappa' C_2 \cosh(\kappa' x_3)}{1 + \alpha \frac{x_3}{L}}. \quad (19)$$

From Eq. (10), the electrical potential function can be achieved as

$$\varphi = \frac{\kappa' C_1 \sinh(\kappa' x_3) + \kappa' C_2 \cosh(\kappa' x_3)}{(n_0' \frac{\mu_{33}^{nr}}{D_{33}^{nr}} + p_0' \frac{\mu_{33}^{pr}}{D_{33}^{pr}})(1 + \alpha \frac{x_3}{L})} + C_3. \quad (20)$$

After that, the variation of electron concentrations can be derived further by utilizing the first equation of Eq. (9):

$$\Delta n = n_0' \frac{\mu_{33}^{nr}}{D_{33}^{nr}} \frac{\kappa' C_1 \sinh(\kappa' x_3) + \kappa' C_2 \cosh(\kappa' x_3)}{(n_0' \frac{\mu_{33}^{nr}}{D_{33}^{nr}} + p_0' \frac{\mu_{33}^{pr}}{D_{33}^{pr}})(1 + \alpha \frac{x_3}{L})} + n_0' \frac{\mu_{33}^{nr}}{D_{33}^{nr}} C_3 + C_4. \quad (21)$$

Combining Eqs. (19) and (21), we have:

$$\begin{aligned}\Delta p &= n_0' \frac{\mu_{33}^{nr}}{D_{33}^{nr}} \frac{\kappa' C_1 \sinh(\kappa' x_3) + \kappa' C_2 \cosh(\kappa' x_3)}{(n_0' \frac{\mu_{33}^{nr}}{D_{33}^{nr}} + p_0' \frac{\mu_{33}^{pr}}{D_{33}^{pr}})(1 + \alpha \frac{x_3}{L})} + n_0' \frac{\mu_{33}^{nr}}{D_{33}^{nr}} C_3 \\ &\quad + C_4 - \frac{\kappa' C_1 \sinh(\kappa' x_3) + \kappa' C_2 \cosh(\kappa' x_3)}{1 + \alpha \frac{x_3}{L}},\end{aligned}\quad (22)$$

which can lead to

$$u_3 = \frac{-F}{\bar{c}_{33}' A_0 (1 + \alpha \frac{x_3}{L})} \frac{L - \bar{e}_{33}'}{\bar{c}_{33}'} \frac{\kappa' C_1 \sinh(\kappa' x_3) + \kappa' C_2 \cosh(\kappa' x_3)}{(n_0' \frac{\mu_{33}^{nr}}{D_{33}^{nr}} + p_0' \frac{\mu_{33}^{pr}}{D_{33}^{pr}})(1 + \alpha \frac{x_3}{L})} - \frac{\bar{e}_{33}'}{\bar{c}_{33}'} C_3 + C_5. \quad (23)$$

Similarly, for the region $x_3 \leq 0$, the fields are:

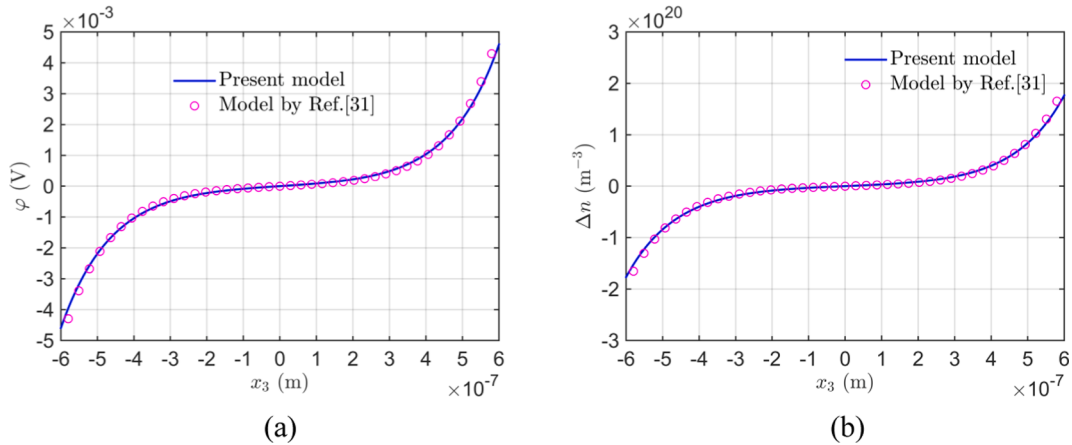


Fig. 2. A comparison of the present results with the results in Ref. [31]. (a) Electric potential function, (b) Electron concentration perturbation.

C_1, C_2, \dots, C_{10} are ten unknown constants that need to be determined after considering the boundary conditions at the two ends $x_3 = \pm L$ and the continuity conditions at the interface $x_3 = 0$. At $x_3 = \pm L$, the boundary conditions are:

$$A\sigma_{33}(\pm L) = F, AD_3(\pm L) = 0, AJ_3^n(\pm L) = AJ_3^p(\pm L) = 0. \quad (25)$$

The continuity conditions at $x_3 = 0$ requires

$$\begin{aligned} A\sigma_{33}(0^+) &= A\sigma_{33}(0^-), AD_3(0^+) = AD_3(0^-), AJ_3^n(0^+) = AJ_3^p(0^-), \\ u_3(0^+) &= u_3(0^-), \quad \varphi(0^+) = \varphi(0^-), \\ n(0^+) &= n(0^-), \quad p(0^+) = p(0^-). \end{aligned} \quad (26)$$

It should be stressed that the boundary conditions $A\sigma_{33}(\pm L) = F$ and $AJ_3^n(\pm L) = AJ_3^p(\pm L) = 0$ have been satisfied in Eqs. (9) and (12). Meanwhile, the continuity conditions $A\sigma_{33}(0^+) = A\sigma_{33}(0^-)$ and $AJ_3^n(0^+) = AJ_3^p(0^-)$ are also automatically satisfied. To uniquely determine the arbitrary constants in the mechanical displacement and the electric potential, we may set [19,31]:

$$\varphi(0) = 0, u_3(0) = 0. \quad (27)$$

Up to now, we have nine available conditions in Eq. (25), (26) and (27). In addition, the total electrons and holes after the formation of PN junction should be the same as their initial values, which requires:

$$\int_{-L}^L A\Delta n dx = 0, \int_{-L}^L A\Delta p dx = 0. \quad (28)$$

Actually, the two expressions in Eq. (28) are correlative, and only one of them is independent.

Utilizing the boundary conditions, continuity conditions and conservation conditions mentioned above, the ten linear algebraic equations can be solved numerically, and the electromechanical fields in a PS PN junction with variable cross sections can be analytically achieved.

4. Numerical results and discussion

As a typical example, the material of the n-type and p-type PS fiber is chosen as wurtzite ZnO, which is commonly used to fabricate PS devices. For a homogeneous junction, the material is uniform and the c -axis of the crystal is along the x_3 -axis. Meanwhile, for a heterogeneous junction, the c -axis of the right region is reversed, just like the work in Refs. [17,33]. The length of the PN junction is $2L = 3 \mu\text{m}$ with the material constants of ZnO from Ref. [31]. During the following analysis, a simple doping profile is given by $p_0^l = n_0^r = 10^{21} \text{ m}^{-3}$, and $p_0^r = n_0^l = 7 \times 10^{20} \text{ m}^{-3}$ unless otherwise stated. For convenience, the section areas of the two end faces $x_3 = \pm L$ are marked as A_1 .

4.1. Numerical validation

Before numerical analysis, it is necessary to validate the theoretical results of a non-uniform PS PN junction derived above. Considering this, we set $L = 0.6 \mu\text{m}$, $n_0^l = n_0^r = 10^{21} \text{ m}^{-3}$, $p_0^l = p_0^r = 0$, $a^l = a^r = 0$ and $A_0 = 2.598 \times 10^{-14} \text{ m}^{-2}$, which means that the PN junction is transformed to a single doped n-type PS fiber with a constant cross section as in Ref. [31]. When a pair of forces $F = 8.5 \text{ nN}$ are applied, the distributions of electric potential function φ and electron concentration perturbation Δn calculated via the present method are demonstrated in Fig. 2, as well as those from Ref. [31]. The curves match very well with each other, indicating that the present theoretical model has a high calculation accuracy to analyze the electromechanical fields in a PS PN junction.

4.2. The influence of cross area variation

To investigate the influence of cross area variation on the PS PN junction, some electromechanical fields including electric potential function φ , electric field E_3 , strain S_3 , and mechanical displacement u_3 near the interface of a homogeneous junction and a heterogeneous junction when $F = 0$ are depicted and shown in Fig. 3. Here, A_1 is kept constant to be $2.598 \times 10^{-14} \text{ m}^{-2}$ and A_0 is variable. $d_0 > d_1$ stands for a bulge profile and $d_0 < d_1$ represents a concave one. Fig. 3(a), 3(c), 3(e), and 3(g) belong to the homogenous junction and Fig. 3(b), 3(d), 3(f) and 3(h) are corresponding to the heterogeneous junction. Since the fields near $x_3 = \pm 1 \mu\text{m}$ have already stabilized, only the region within $|x_3| < 1 \mu\text{m}$ is shown. As known from the semiconductor theory [15], for a uniform PS PN junction with traction free, the junction properties, e.g., the height and width of the space charge region, are only dependent on carrier concentrations and material properties. However, electromechanical fields in a non-uniform PS PN junction are also related to its geometric parameter, especially for a concave profile with $d_0 < d_1$ in Fig. 3. In Fig. 3(a), 3(b), 3(c), and 3(d), a shrinking cross section at the interface leads to a narrow depletion layer width and a stronger electric field, and the fields distributions for a homogeneous junctions are similar to those for heterogeneous junctions. However, for the mechanical fields in Fig. 3(e), 3(f), 3(g) and 3(h), their distributions in the n-type part of heterogeneous junctions are opposite to those in homogeneous junctions, which is induced by the reversed c -axis.

4.3. The working performance comparison between homogeneous and heterogeneous junctions

When a pair of axial mechanical forces are applied at the two ends of the non-uniform PS PN junction, the induced electromechanical fields accompanied by acoustic waves may be different from those in the

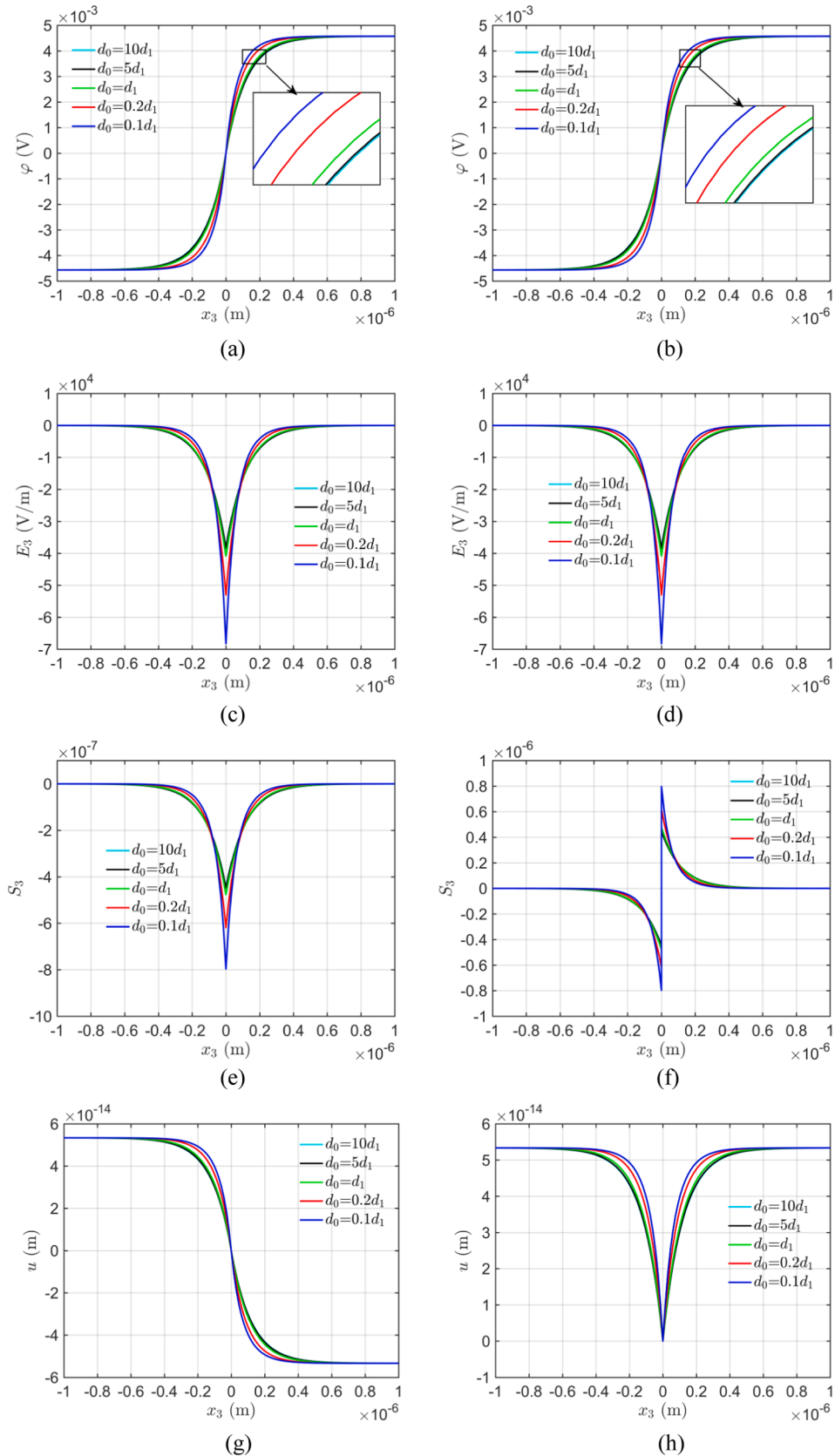


Fig. 3. Electromechanical fields for different diameters at the interface. (a), (c), (e), and (g) are respectively the electric potential function φ , electric field E_3 , strain S_3 , and mechanical displacement u_3 for a uniform c-axis, and (b), (d), (f) and (h) are those fields for an opposite c-axis.

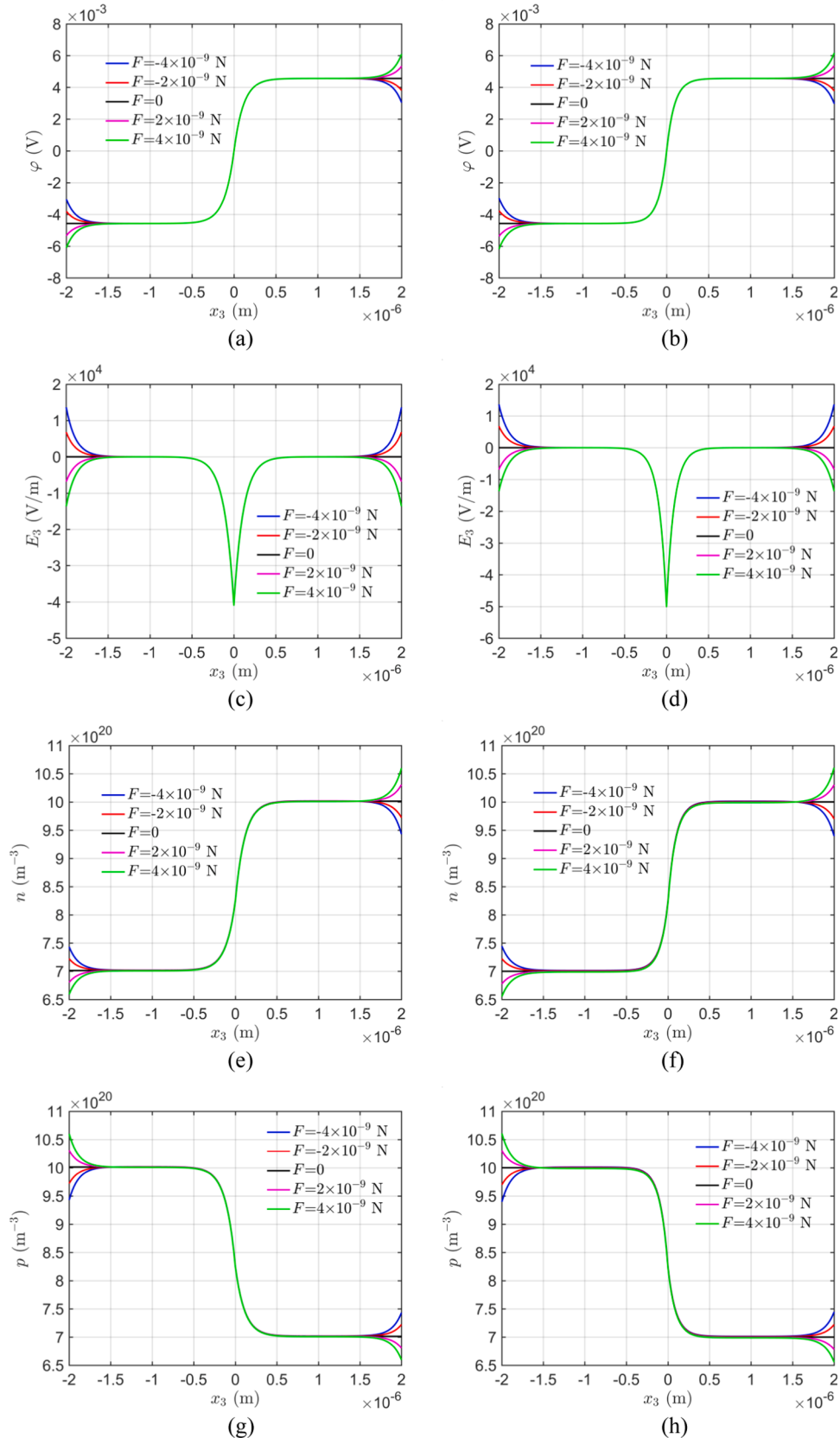


Fig. 4. Electromechanical fields of homogeneous PS PN junctions for different values of F . (a), (c), (e), (g), (i) and (k) respectively stand for the distributions of the electric potential function φ , electric field E_3 , electron concentration n , hole concentration p , strain S_3 , and electric displacement D_3 of a uniform PN junction with a constant cross section, and (b), (d), (f), (h), (j) and (l) are those fields for the case of a variable cross section.

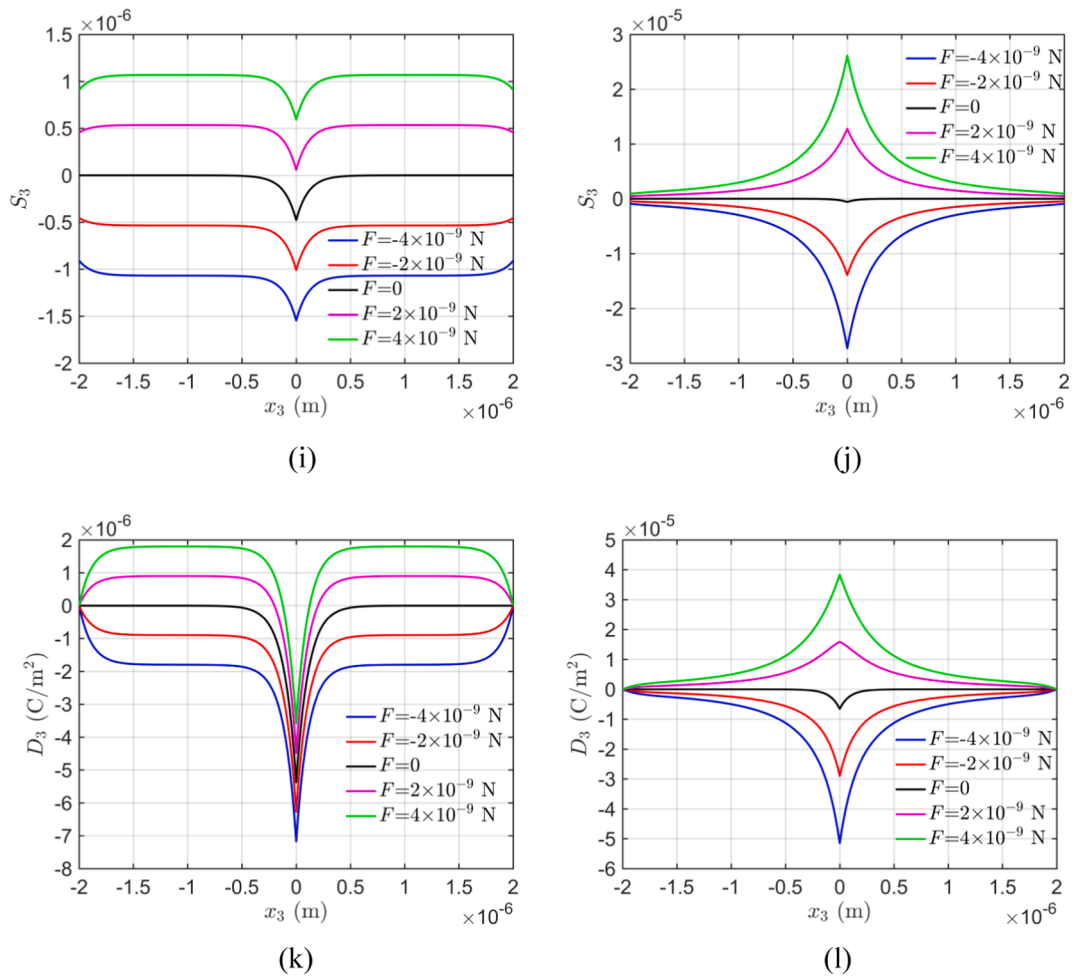


Fig. 4. (continued).

uniform junction. In order to demonstrate the working performance of PS devices, we compare the electromechanical fields respectively in a uniform and non-uniform homogeneous PS PN junction with the diameter ratio of $5d_0 = d_1$ under different values of applied force F , such as in Fig. 4. Again, A_1 is kept as $2.598 \times 10^{-14} \text{ m}^{-2}$ and A_0 is variable. Performances of the uniform and the non-uniform PS PN junctions in Fig. 4(a) – 4(h) are similar. When axial forces are applied at the two ends of the homogeneous junction, the electric potential function φ , electric field E_3 , electron concentration distribution n and hole concentration distribution p change rapidly near the two ends and almost keep stable in the middle region due to the screen effect of free carriers, which is in accordance with the results in Ref. [20]. Furthermore, comparing figures in the left and the right column, it can be concluded that the influence caused by the cross section area variation seems trivial. However, in Fig. 4(i), 4(j), 4(k) and 4(l), it becomes more prominent. Fig. 4(i) indicates that the strain is almost constant in the most part of the uniform fiber. Meanwhile, the uniform junction in the middle part always tends to shrink regardless of the sign of F , which is because the electric field in this region is always negative and shrinks the fiber via piezoelectric effect, such as Fig. 4(c). Nevertheless, for a non-uniform junction in Fig. 4(j), the strain always varies along x_3 and the thinner part possesses larger strain as anticipated, which furthermore induces more polarization and larger electric displacement distributions, such as Fig. 4(k) and 4(l).

Beyond of electromechanical fields of homogeneous PS PN junctions, we also investigate the heterogeneous PS PN junctions, with the results shown in Fig. 5. All parameters here are the same as those in Fig. 4 except the reversed c -axis of the n-type region. Comparing Figs. 5 and 4, we may notice that fields near the interface in heterogeneous junctions are more sensitive to the external applied forces, including the constant cross sections and variable cross sections, which is also the reason that a heterogeneous PS PN junction is preferred to manipulate the current [18,23]. Especially, in Fig. 5(b), with the magnitude increase (decrease) of F , a potential barrier (well) appears at the interface, whose height (depth) is a key parameter for the current adjustment and control. Actually, the potential barrier (well) also appears in Fig. 5(a) for a uniform junction. However, it is too tiny to be observed. This phenomenon demonstrates that PS PN junctions with variable cross sections may be more advantages in current manipulation than those with constant cross sections. In any case, however, potential barriers and wells are more likely to appear in heterogeneous junctions than in homogeneous junctions, which will be explained later. Because of these potential barriers and wells, the electric fields are discontinuous across the interface as they depend on the gradient of the electric potential. The carrier concentration distributions are not plotted here since they look very like the potential distributions. Unlike Fig. 4(i) and 4(j), the strains in 5(e) and 5(f) are not continuous at the interface, which is caused by the reversed c -axis of the n-zone. For the homogeneous junctions, the c -

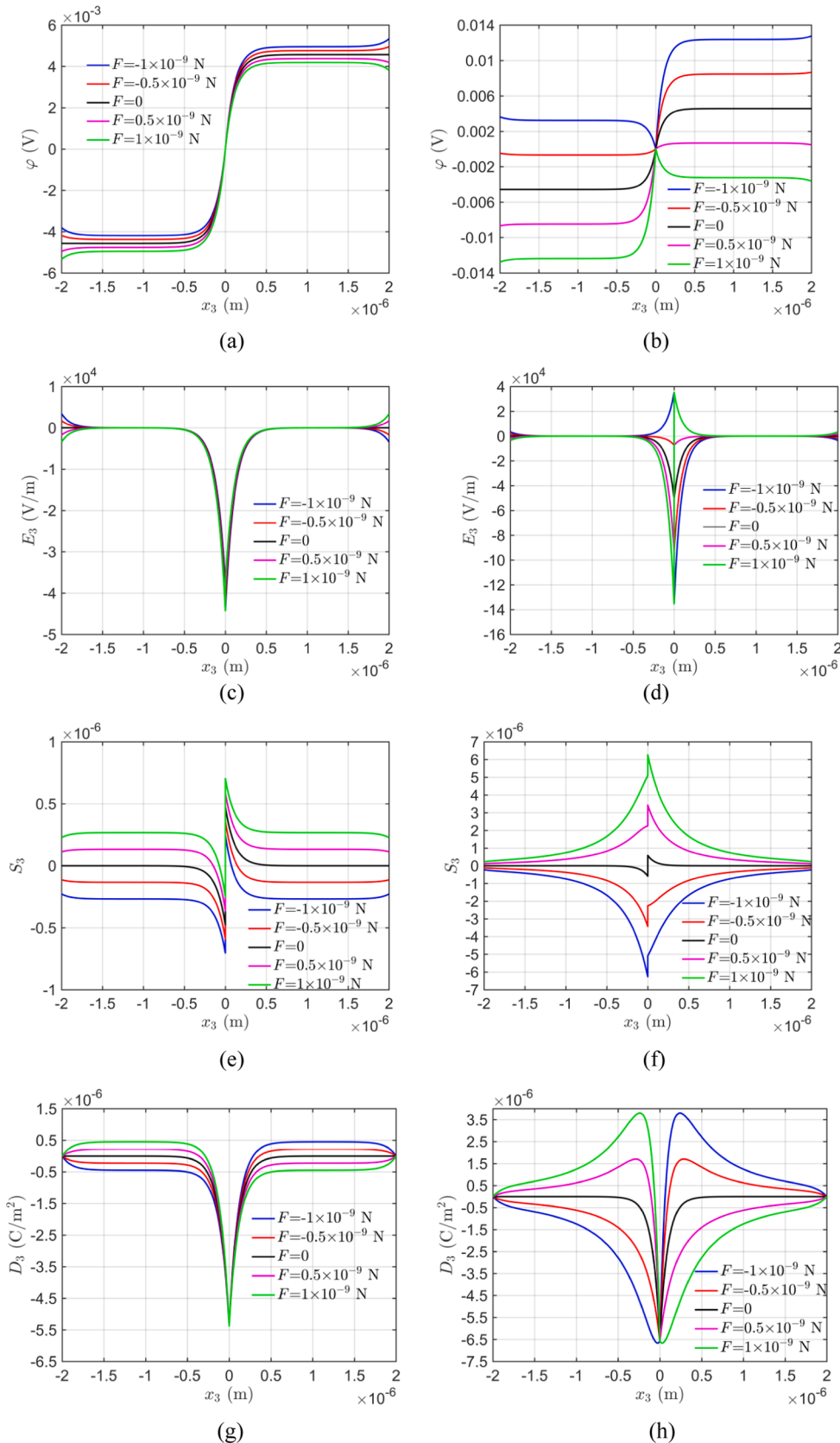


Fig. 5. Electromechanical fields of heterogeneous PS PN junctions for different values of F . (a), (c), (e) and (g) respectively stand for the distributions of the electric potential function φ , electric field E_3 , strain S_3 , and electric displacement D_3 of a uniform PN junction with a constant cross section, and (b), (d), (f) and (h) are those fields for the case of a variable cross section.

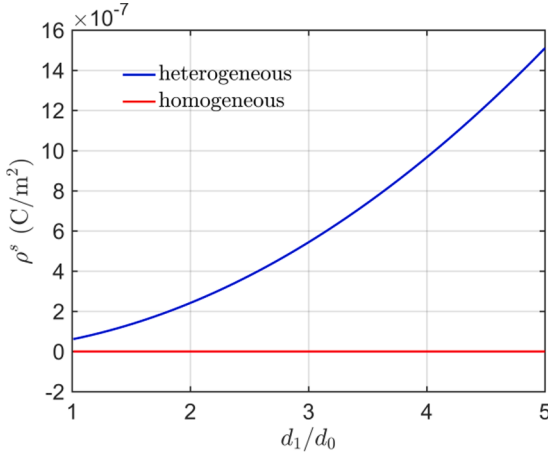


Fig. 6. Interface polarization charge density ρ^s versus the diameter ratio d_1/d_0 .

axis of the two halves is in the same direction, and then the negative electric field shown in Fig. 4(c) will stretch or compress both sides of the interface at the same time via piezoelectric effect. However when it comes to the heterogeneous junctions whose *c*-axes reverse at the interface, the negative electric field in Fig. 5(c) tends to stretch one side of the fiber while compressing the other, which leads to the strain discontinuity. As expected, the electric displacement in Fig. 5(h) varies more rapidly in the thinner part of the junction, and its sign is related to

the poling direction of the two regions.

The difference of the potential distributions near the interface between homogeneous and heterogeneous junctions can be explained by the interface polarization charge density ρ^s . It can be calculated from Ref. [17], i.e.,

$$P_3 = D_3 - \epsilon_0 E_3, \quad \rho^s = P_3(0^-) - P_3(0^+), \quad (29)$$

with P_3 representing the axial electric polarization. The ρ^s variation versus the diameter ratio d_1/d_0 for homogeneous and heterogeneous junctions are illustrated in Fig. 6 when $F = 1$ nN and d_1 is kept constant. For the homogeneous junction, ρ^s is almost zero for all values of d_1/d_0 , indicating that there is no piezoelectric charge at the interface. Obviously, the electrical field won't be changed. Compared with that, for the heterogeneous junctions, the reversed *c*-axis of the n-type zone leads to a discontinuous P_3 at the interface, resulting in net positive charges and thus changes the potential distributions near the interface.

Fig. 5 indicates that the height (depth) of the potential barrier (well) at the interface of a PS PN junction can be adjusted by the applied end force. In order to explicitly demonstrate their relationship, we define the potential difference between the interface and the stable part of the p-type zone under $F = 0$ as V_D^0 , and their potential difference when $F > 0$ as \bar{V} . Therefore, the dependences of $\bar{V} = V_D/V_D^0$ upon F for homogeneous junctions and heterogeneous junctions with different cross sections can be calculated and depicted in Fig. 7(a) and 7(b). Meanwhile, \bar{V} versus the diameter ratio d_1/d_0 for homogeneous junctions and heterogeneous junctions when F is kept as 1 nN is also plotted in Fig. 7(c). In Fig. 7(a)

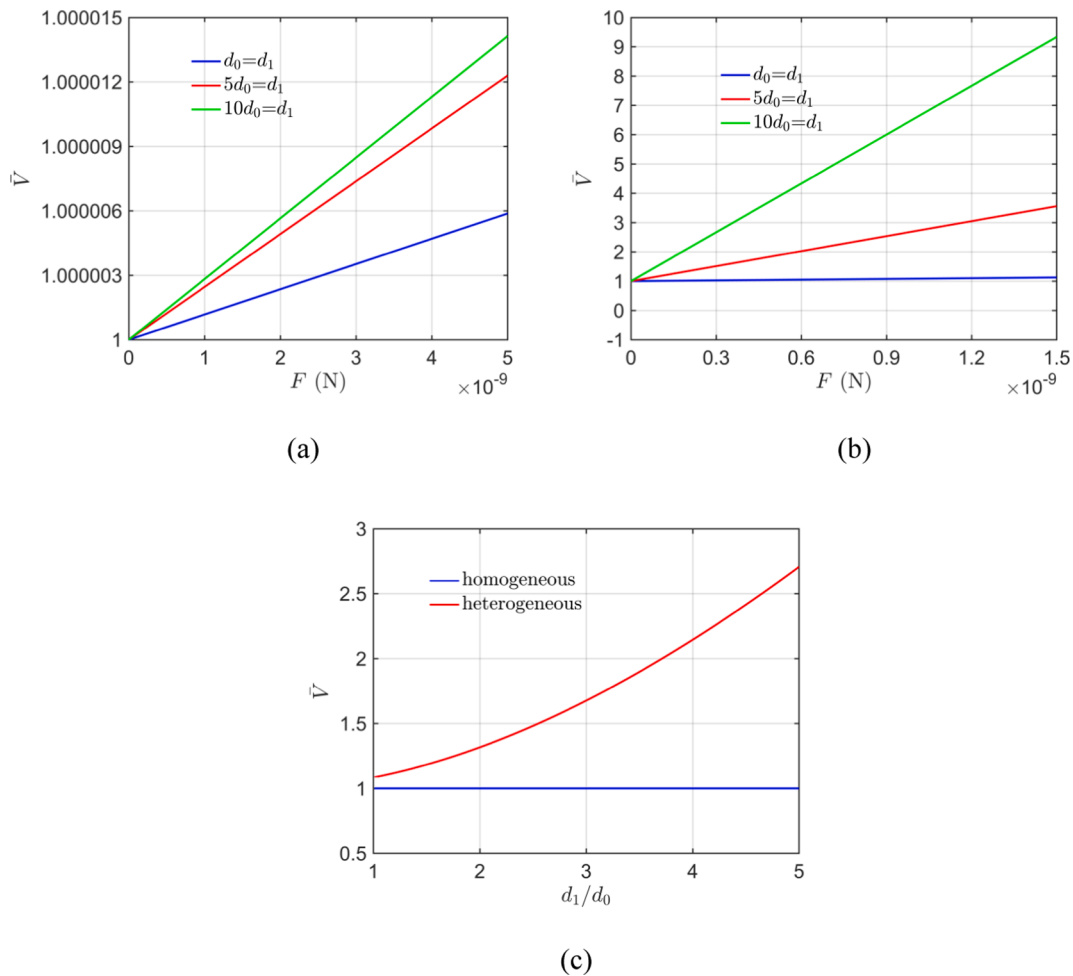


Fig. 7. The potential difference \bar{V} versus: (a) the applied end forces F in a homogeneous junction; (b) the applied end forces F in a heterogeneous junction; (c) the diameter ratio d_1/d_0 when $F = 1$ nN.

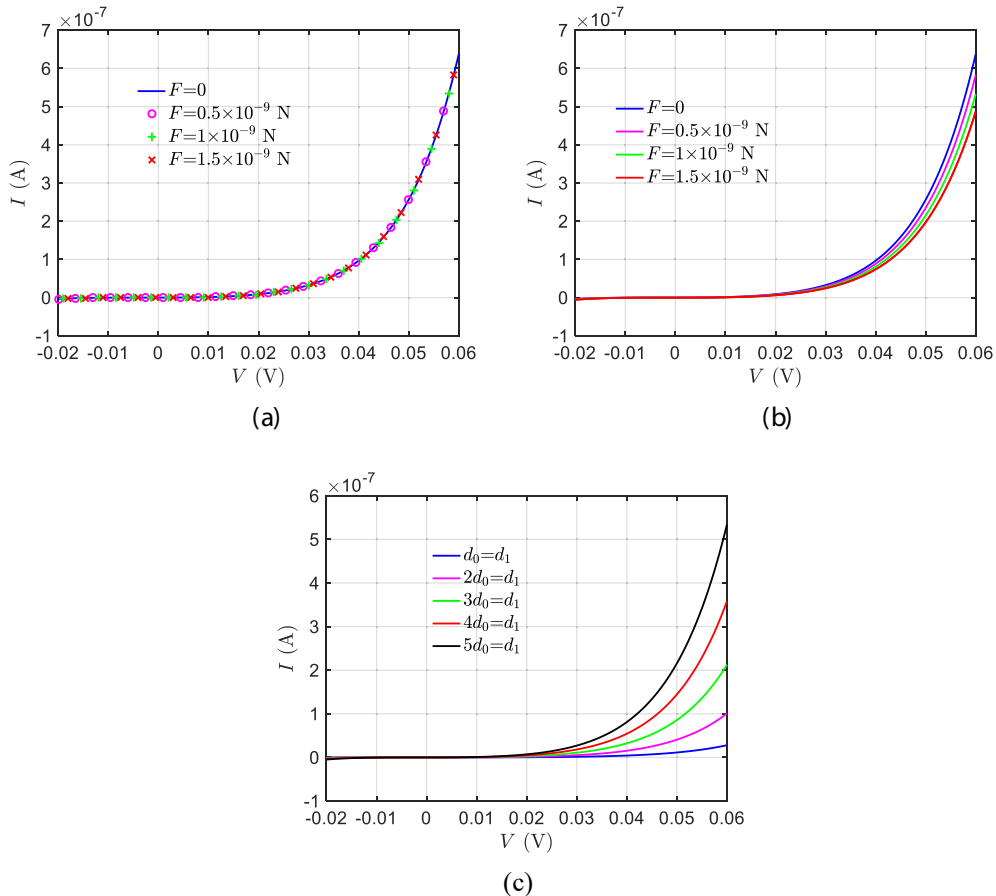


Fig. 8. I - V curves respectively for a homogeneous junction with $5d_0 = d_1$ (a), heterogeneous junction with $5d_0 = d_1$ (b), and heterogeneous junction with $F = 1$ nN (c).

for the homogeneous junction, \bar{V} increases with the rise of F with a very tiny magnitude, which also coincides with Fig. 4(a) and 4(b). By contrast, in Fig. 7(b) for the heterogeneous junction, \bar{V} increases rapidly with the value much larger than that in Fig. 7(a). As expected, Fig. 7(c) looks much similar to Fig. 6, demonstrating the potential change near the interface is induced by the net piezoelectric charges. In addition, a smaller d_0 will lead to a faster increment of \bar{V} . Therefore, a heterogeneous PS PN junction is more suitable to work as a mechanical gated transistor since the potential barrier height (well depth) can be controlled much more easily. Furthermore, a thinner and necking junction leads to a higher manipulation efficiency, which is beneficial for the piezotronic device design. In addition, we note that all the conclusions above are obtained based on the linearized model. To prove its accuracy, we compare some results with the nonlinear one-dimensional model in COMSOL Multiphysics software, and details are shown in the Appendix.

As circuit elements concerned, the current-voltage relation (I - V curves) of PN junctions is discussed finally. Considering the I - V relation is strongly nonlinear, a COMSOL analysis is performed using the nonlinear current constitutive relations. The electrical boundary conditions applied at the two ends of the PS PN junction is:

$$\varphi(-L) = V, \varphi(L) = -V, \quad (30)$$

and the results for the homogeneous junctions when $5d_0 = d_1$ are shown in Fig. 8(a). As expected, the I - V curves are not sensitive to the applied end force. For the heterogeneous junctions, I - V curves for different

values of F and diameter ratios are also plotted in Fig. 8(b) and 8(c), respectively. It shows that the current-voltage relations are controlled by the applied end force F and the fiber diameter, which are also consistent with the conclusions obtained in previous sections.

5. Conclusions

Totally speaking, the modulation of a piezoelectric semiconductive PN junction with variable cross sections is analyzed from the views of theoretical analysis and numerical simulations, with the electromechanical fields of piezoactive acoustic wave and current-voltage relations demonstrated in detail. The analytical solutions of the fields in homogeneous and heterogeneous junctions are obtained and compared under the framework of the linearized one-dimensional model. The governing equation with variable coefficients is transformed to a commonly used Helmholtz equation for a selected area variation function. The results obtained by this linearized analytical model are validated via the comparison with those from the FEM software COMSOL Multiphysics, and some conclusions can be summarized as follows:

- (1) The electrical fields of in heterogeneous PS PN junctions are more sensitive to the cross section area variation than those in homogeneous junctions. The height of the produced potential barrier in a heterogeneous junction reaches up to approximate 2.7 times than that in a homogeneous one.

- (2) The current–voltage relations of a heterogeneous PS PN junction can be manipulated by piezoelectric fields more conveniently in a non-uniform necking fiber. When applied voltage is 0.06 V, the current flow through a non-uniform junction with diameter ratio of 5 is almost 10 times than that through a uniform one.

The theoretical and numerical results reported herein not only clarify some key issues in piezotronic devices, such as the current regulation, heterogeneous junction, potential barrier, and so forth, but also provide a new methodology, i.e., variable cross-section, to produce high-sensitivity devices.

Declaration of Competing Interest

The authors declare that they have no known competing financial interests or personal relationships that could have appeared to influence the work reported in this paper.

Acknowledgements

This work was supported by the National Natural Science Foundation of China (12172171, 12061131013 and 11972276), the State Key Laboratory of Mechanics and Control of Mechanical Structures at NUAA (No. MCMS-E-0520K02), the Fundamental Research Funds for the

Central Universities (NE2020002 and NS2019007), National Natural Science Foundation of China for Creative Research Groups (No. 51921003), National Natural Science Foundation of Jiangsu Province (BK20211176), Postgraduate Research & Practice Innovation Program of Jiangsu Province (KYCX21_0179), Local Science and Technology Development Fund Projects Guided by the Central Government (2021Szvup061), the Start-up Fund supported by NUAA, and a project funded by the Priority Academic Program Development of Jiangsu Higher Education Institutions (PAPD). Prof. Iren E. Kuznetsova and Dr. Vladimir Kolesov thank Russian Ministry of Science and Higher Education (Agreement #13.1902.21.0010) for financial support.

Appendix

In this appendix, we show some comparisons of the analytical solutions with those obtained from the nonlinear one-dimensional model in COMSOL Multiphysics software. Only the fields in the heterogeneous junction when $F = 1$ nN are plotted since they vary the most dramatically in Figs. 4 and 5. It can be observed that the field distributions using the linearized model agree well with those calculated by COMSOL, which indicates the validity of the derived linearized analytical solutions.

Fig. A1

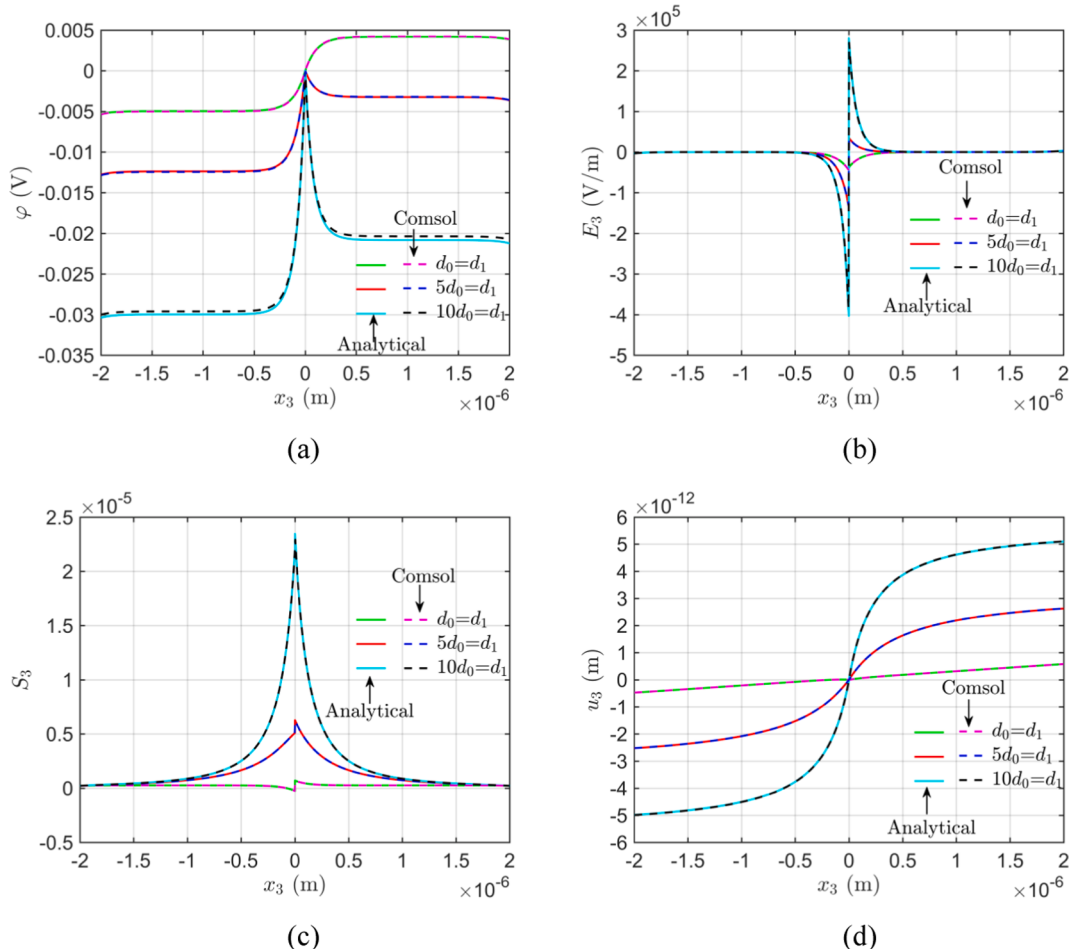


Fig. A1. Comparisons of linear analytical and nonlinear numerical solutions at a heterogeneous junction for $F = 1$ nN: (a) Electric potential φ , (b) Electric field E_3 , (c) Strain S_3 , and (d) Mechanical displacement u_3 .

References

- [1] Z.L. Wang, W.Z. Wu, C. Falconi, Piezotronics and piezo-photronics with third-generation semiconductors, *MRS Bull.* 43 (12) (2018) 922–927.
- [2] W.G. Hu, C. Zhang, Z.L. Wang, Recent progress in piezotronics and tribotronics, *Nanotechnology* 30 (4) (2019), 042001.
- [3] R. Araneo, G. Lovat, P. Burghignoli, C. Falconi, Piezo-Semiconductive Quasi-1D Nanodevices with or without Anti-Symmetry, *Adv. Mater.* 24 (34) (2012) 4719–4724.
- [4] P.A. Mante, Y.R. Huang, S.C. Yang, T.M. Liu, A.A. Maznev, J.K. Sheu, C.K. Sun, THz acoustic phonon spectroscopy and nanoscopy by using piezoelectric semiconductor heterostructures, *Ultrasonics* 56 (2015) 52–65.
- [5] F.Y. Jiao, P.J. Wei, X.L. Zhou, Y.H. Zhou, The dispersion and attenuation of the multi-physical fields coupled waves in a piezoelectric semiconductor, *Ultrasonics* 92 (2019) 68–78.
- [6] Y. Qin, X.D. Wang, Z.L. Wang, Microfibre-nanowire hybrid structure for energy scavenging, *Nature* 451 (7180) (2008) 809–813.
- [7] M.A. Johar, M.A. Hassan, A. Waseem, J.S. Ha, J.K. Lee, S.W. Ryu, Stable and High Piezoelectric Output of GaN Nanowire-Based Lead-Free Piezoelectric Nanogenerator by Suppression of Internal Screening, *Nanomaterials* 8 (6) (2018) 437.
- [8] X.D. Wang, J. Zhou, J.H. Song, J. Liu, N.S. Xu, Z.L. Wang, Piezoelectric field effect transistor and nanoforce sensor based on a single ZnO nanowire, *Nano Lett.* 6 (12) (2006) 2768–2772.
- [9] R.S. Dahiya, G. Metta, M. Valle, A. Adami, L. Lorenzelli, Piezoelectric oxide semiconductor field effect transistor touch sensing devices, *Appl. Phys. Lett.* 95 (3) (2009), 034105.
- [10] J.J. Qi, H. Zhang, S.N. Lu, X. Li, M.X. Xu, Y. Zhang, High performance indium-doped ZnO gas sensor, *J. Nanomater.* 2015 (2015), 954747.
- [11] J. Zhang, J.L. Zhou, Humidity-dependent piezopotential properties of zinc oxide nanowires: Insights from atomic-scale modelling, *Nano Energy* 50 (2018) 298–307.
- [12] W.Z. Wu, Y.G. Wei, Z.L. Wang, Strain-gated piezotronic logic nanodevices, *Adv. Mater.* 22 (42) (2010) 4711–4715.
- [13] C. Sun, F.D. Wu, Y.Q. Fu, D.J. Wallis, R. Mikhaylov, F. Yuan, D.F. Liang, Z.J. Xie, H. L. Wang, R. Tao, M.H. Shen, J. Yang, W.P. Xun, Z.L. Wu, Z.Y. Yang, H.X. Cang, X. Yang, Thin film Gallium nitride (GaN) based acoustofluidic Tweezer: Modelling and microparticle manipulation, *Ultrasonics* 108 (2020), 106202.
- [14] A.A. Maznev, K.J. Manke, K.H. Lin, K.A. Nelson, C.K. Sun, J.I. Chyi, Broadband terahertz ultrasonic transducer based on a laser-driven piezoelectric semiconductor superlattice, *Ultrasonics* 52 (2012) 1–4.
- [15] S.M. Sze, Physics of Semiconductor Devices, John Wiley&Sons, 1981.
- [16] M.K. Guo, Y. Li, G.S. Qin, M.H. Zhao, Nonlinear solutions of PN junctions of piezoelectric semiconductors, *Acta Mech.* 230 (5) (2019) 1825–1841.
- [17] R.R. Cheng, C.L. Zhang, W.Q. Chen, J.S. Yang, Temperature effects on PN junctions in piezoelectric semiconductor fibers with thermoelastic and pyroelectric couplings, *J. Electron. Mater.* 49 (5) (2020) 3140–3148.
- [18] Y. Liu, Y. Zhang, Q. Yang, S.M. Niu, Z.L. Wang, Fundamental theories of piezotronics and piezo-photronics, *Nano Energy* 14 (2015) 257–275.
- [19] Y.X. Luo, C.L. Zhang, W.Q. Chen, J.S. Yang, An analysis of PN junctions in piezoelectric semiconductors, *J. Appl. Phys.* 122 (20) (2017), 204502.
- [20] S.Q. Fan, W.L. Yang, Y.T. Hu, Adjustment and control on the fundamental characteristics of a piezoelectric PN junction by mechanical-loading, *Nano Energy* 52 (2018) 416–421.
- [21] R. Araneo, C. Falconi, Lateral bending of tapered piezo-semiconductive nanostructures for ultra-sensitive mechanical force to voltage conversion, *Nanotechnology* 24 (26) (2013), 265707.
- [22] P. Amiri, C. Falconi, Fundamental definitions for axially-strained piezo-semiconductive nanostructures, *Micromachines* 12 (1) (2021) 20.
- [23] Y.M. Zhang, G.W. Hu, Y. Zhang, L. Li, M. Willatzen, Z.L. Wang, High performance piezotronic devices based on non-uniform strain, *Nano Energy* 60 (2019) 649–655.
- [24] H.Y. Huang, Z.H. Qian, J.S. Yang, Mechanical manipulation of electrical behaviors of piezoelectric semiconductor nanofibers by time-dependent stresses, *Acta Mech. Solida Sin.* 33 (5) (2020) 579–585.
- [25] P. Li, F. Jin, J.S. Yang, Effects of semiconduction on electromechanical energy conversion in piezoelectrics, *Smart Mater. Struct.* 24 (2) (2015), 025021.
- [26] F.Y. Jiao, P.J. Wei, Y.H. Zhou, X.L. Zhou, Wave propagation through a piezoelectric semiconductor slab sandwiched by two piezoelectric half-spaces, *Eur. J. Mech. A-Solids* 75 (2019) 70–81.
- [27] N. Li, Z.H. Qian, J.S. Yang, Effects of edge and interior stresses on electrical behaviors of piezoelectric semiconductor films, *Ferroelectrics* 571 (1) (2021) 96–108.
- [28] J. Gao, Y. Lyu, M.F. Zheng, M.K. Liu, H.Y. Liu, B. Wu, C.F. He, Modeling guided wave propagation in functionally graded plates by state-vector formalism and the Legendre polynomial method, *Ultrasonics* 99 (2019), 105953.
- [29] B.R.F. Pierret, Semiconductor Fundamentals, Addison-Wesley, 1989.
- [30] H.F. Tiersten, Linear Piezoelectric Plate Vibrations, *Linear Piezoelectric Plate Vibration* (1969).
- [31] C.L. Zhang, X.Y. Wang, W.Q. Chen, J.S. Yang, An analysis of the extension of a ZnO piezoelectric semiconductor nanofiber under an axial force, *Smart Mater. Struct.* 26 (2) (2017), 025030.
- [32] G.L. Wang, J.X. Liu, X.L. Liu, W.J. Feng, J.S. Yang, Extensional vibration characteristics and screening of polarization charges in a ZnO piezoelectric semiconductor nanofiber, *J. Appl. Phys.* 124 (9) (2018), 094502.
- [33] G.Y. Yang, L. Yang, J.K. Du, J. Wang, J.S. Yang, PN junctions with coupling to bending deformation in composite piezoelectric semiconductor fibers, *Int. J. Mech. Sci.* 173 (2020), 105421.
- [34] C. Ren, K.F. Wang, B.L. Wang, Adjusting the electromechanical coupling behaviors of piezoelectric semiconductor nanowires via strain gradient and flexoelectric effects, *J. Appl. Phys.* 128 (21) (2020), 215701.
- [35] C.L. Zhang, X.Y. Wang, W.Q. Chen, J.S. Yang, Carrier distribution and electromechanical fields in a free piezoelectric semiconductor rod, *J. Zhejiang Univ.-Sci. A* 17 (1) (2016) 37–44.
- [36] K. Fang, Z.H. Qian, J.S. Yang, Piezopotential in a composite cantilever of piezoelectric dielectrics and nonpiezoelectric semiconductors produced by shear force through c(15), *Mater. Res. Express* 6 (11) (2019), 115917.
- [37] S. Abrate, Vibration of non-uniform rods and beams, *J. Sound Vib.* 185 (4) (1995) 703–716.